2011 NDIA GROUND VEHICLE SYSTEMS ENGINEERING AND TECHNOLOGY SYMPOSIUM
MODELING & SIMULATION, TESTING AND VALIDATION (MSTV) MINI-SYMPOSIUM
AUGUST 9-11 DEARBORN, MICHIGAN

EXPERIMENTAL VALIDATION OF A MULTIBODY DYNAMICS MODEL OF THE SUSPENSION SYSTEM OF A TRACKED VEHICLE

Tamer M. Wasfy
Advanced Science and Automation Corp.
Indianapolis, IN

James O'Kins and David Ryan
U.S. Army Tank Automotive Research
Development and Engineering Center
Warren, MI

ABSTRACT

A time-accurate multibody dynamics model of the suspension system of a tracked vehicle is experimentally validated using a full-scale tracked-vehicle on an N-post motion simulator. The experiments consist of harmonic excitations at various amplitudes and frequencies and ramp excitations of the vehicle road-wheels (without the track), with each road wheel under one linear actuator of the N-post motion simulator. A high-fidelity multibody dynamics model of the vehicle along with the N-post motion simulator is constructed. The multibody dynamics model consists of rigid bodies, joints, rotational springs (that include non-linear rotational stiffness, damping and friction), actuators and contact surfaces. The rigid bodies rotational equations of motion are written in a body-fixed frame with the total rigid-body rotation matrix updated each time step using incremental rotations. Connection points on the rigid bodies are used to define joints between the bodies including revolute, cylindrical, prismatic and bracket joints. A penalty model is used to impose the joint and normal contact constraints. The contact model detects contact between discrete points on the surface of each wheel (master contact surfaces) and a polygonal surface representation of the linear actuators dishpans (slave contact surfaces). A recursive bounding box/bounding sphere contact search algorithm is used to allow fast contact detection. An asperity friction model is used for the contact friction forces. The governing equations of motion are solved along with joint/constraint equations using a time-accurate explicit solution procedure. The time-histories of the suspension system rotational deflections are experimentally measured for the various input motion excitations. The experimental measurements are compared with the results predicted using the computational model. The comparison shows that the model can predict with reasonably good accuracy the test tracked-vehicle's dynamic response.

1. INTRODUCTION

Tracked vehicles are used in civilian and military off-road ground vehicles. Tracks have better mobility characteristics than tires on off-road and slippery terrains. This includes:

- Better traction over firm terrains (such as pavement) that is highly sloped or slippery (e.g. wet/icy pavement).
- Better traction and mobility over soft terrains such as snow, sand, and mud.
- Better positive/negative obstacle crossing capability. Tracked vehicles can go over larger obstacles than equivalent wheeled vehicles. Typical obstacles that ground vehicles are tested against include semi-circular and trapezoidal bumps/potholes.

Tracks can be used on vehicles of various sizes ranging from large tractors and excavator to small unmanned ground vehicles. Tracks can also be used in conjunction with tires in order to improve the vehicle's mobility. Tracks can be divided into two types:

- Continuous belt track. The cross-section of a continuous belt track is similar in construction to a tire. It consists of a rubber matrix reinforced with steel, Kevlar and/or polyester wire/ply along the length and width of the track.

Unclassified: Distribution Statement A. Appropriate for public release; distribution is unlimited.

- Segmented track. The track consists of rigid or flexible segments connected using revolute joints. For rigid segmented tracks, the segments are made of steel with a rubber layer on the track-road contact surfaces. Flexible segmented tracks have both reinforced rubber and steel segments. The rubber segments are used for contact between the track and the terrain. The steel segments are used to connect the rubber segments.

Tracked vehicles are flexible multibody systems involving frictional contact, large rotations and large deflections (of the flexible track). A review of flexible multibody dynamics modeling techniques including deformation reference frames, treatment of large rotations, discretization techniques, finite elements, constraint and contact modeling, and solution techniques is presented in [1]. A review of tracked vehicles models was presented in [2]. A finite element multibody dynamics model for tracked vehicles, that can handle both flexible belt-type tracks and rigid segmented tracks, was presented in [2]. The model uses the following computational techniques/elements:

- Explicit time-integration solver accurate for long simulation times [3].
- The algorithm that is used to account for a rigid body rotational motion [4] uses the total rotation matrix relative to the inertial frame to measure the rotation the rigid bodies. This avoids singularity problems associated with 3 and 4 parameter rotation measures. Rigid body rotational equations of motion are written in a body (material) frame. Thus, the inertia tensor is constant. The equations of motion are integrated to yield the incremental rotations angles. The total body rotation matrix is updated using the rotation matrix corresponding to the incremental rotations angles.
- Penalty formulation for modeling joint constraints including spherical, revolute, cylindrical and prismatic joints [4].
- Normal contact modeled using a penalty formulation [5, 6].
- Frictional contact modeled using an accurate and efficient asperity-based friction model [7].
- General contact search algorithm for finding the contact penetration between finite elements and other elements as well as general triangle and quadrilateral surfaces [2].
- Total-Lagrangian spring, truss, beam and solid nonlinear finite elements with Cartesian coordinate degrees of freedom [3, 8-10]. This allows arbitrarily large element rotations with no solution drift due to the use of displacement increments. The element DOFs are referenced to a global inertial reference frame.
- The thin beam elements use a torsional-spring formulation with 3-nodes per element [3, 8] for modeling the bending behavior of the beams.
- 8-node natural deformation modes brick solid elements are used [9, 10]. Those elements can also be used to model shells and beams. One element through the thickness is sufficient to accurately model the membrane, shear, and bending characteristics. The brick elements do not exhibit locking or spurious modes (widely used techniques to alleviate locking such as hourglass control lead to elements that do not maintain solution accuracy over very long solution times). Any material law can be used with those elements including: linear elastic, hyper-elastic, and non-linear laws. Those elements are used to model the rubber matrix of the continuous belt-type tracks. The track reinforcements for those tracks can be modeled using the thin beam torsional-spring element.
- Linear/rotational suspension springs that can include a prescribed non-linear force-deflection relation, a force-deflection rate relation and a friction coefficient-deflection rate relation.

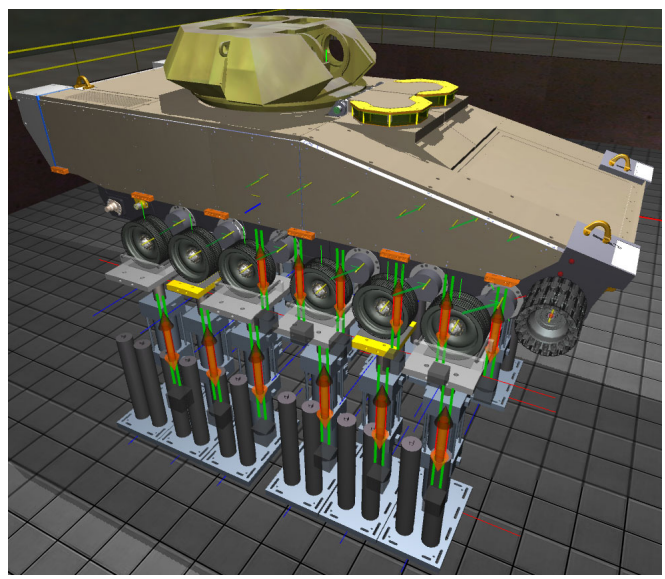

Figure 1. Tracked vehicle on the n-post motion simulator.

The purpose of this paper is to partially experimentally validate the tracked vehicle model presented in [2]. The experimental validation was carried out using a full-scale tracked vehicle that was instrumented and mounted, with the track removed, on an n-post motion simulator (Figure 1). The n-post motion simulator consists of hydraulic linear

Unclassified: Distribution Statement A. Appropriate for public release; distribution is unlimited.

actuators under each road wheel that can be independently controlled to simulate typical road maneuvers that the vehicle is subjected to such as going over bumps/potholes. The time-histories of the angular deflections of the road arms are measured for various input motion excitations. The experiments were used to tune the force – angular velocity relation (damping) of the road arms torsion bars. The results of the experiments are then compared with the results predicted using the computational model.

In addition, in this paper typical simulations of tracked vehicles that can be performed using the present model are also presented. Also, a lumped parameters thick spatial beam element is presented. The element has two rigid body type nodes with each node having 3 translational DOFs and the rotation matrix is used to measure the spatial rotation of the node. The element models each response component independently using simpler sub-elements that include: three mutually orthogonal linear spring sub-elements for modeling one axial and two shear deformations; three mutually orthogonal torsional spring elements for modeling one torsional and two bending deformations of the element. This beam element can be used to model both segmented and continuous tracks.

The rest of this paper is organized as follows. In Section 2 the translational and rotational semi-discrete equations of motion are presented. In Section 3 the finite element formulation for the truss, thin beam, thick beam and solid brick elements are presented. In Section 4 the frictional contact techniques, including penalty formulation for normal contact, asperity friction model and contact search algorithm, are presented. In Section 5 the penalty algorithm for imposing joint constraints is presented. In Section 6, the overall explicit solution algorithm is outlined. In Section 7, the experimental setup is presented. In Section 8 the comparison between the experiment and model is presented. In Section 9 typical numerical simulations of tracked vehicles are presented. Finally, in Section 10 concluding remarks are offered.

2. EQUATIONS OF MOTION

In the subsequent equations the following conventions will be used:

- The indicial notation is used.
- The Einstein summation convention is used for repeated subscript indices unless otherwise noted.
- Upper case subscript indices denote node numbers.
- Lower case subscript indices denote vector component number.
- The superscript denotes time.
- A superposed dot denotes a time derivative.

Two types of finite element nodes are used: point particle nodes and rigid body nodes. Point particle nodes have 3 translational DOFs (Degrees of freedom). The algorithm for writing and integrating the equations of motion for spatial rigid bodies using an explicit finite element code was presented in [4]. In this algorithm, a rigid body is modeled using a finite element node located at its center of mass. The node has 3 translational DOFs defined with respect to the global inertial reference frame and a rotation matrix defined also with respect to the global inertial frame. The use of the total body rotation matrix to measure rigid body rotations avoids singularity problems associated with 3 and 4 parameter rotation measures [3].

The translational equations of motion for the nodes are written with respect to the global inertial reference frame and are obtained by assembling the individual node equations. The equations can be written as:

$$M_K \ddot{x}^t_{Ki} = F_{s}{}^t_{Ki} + F_{a}{}^t_{Ki} \tag{1}$$

where t is the running time, K is the global node number (no summation over K; K=1→N where N is the total number of nodes), i is the coordinate number (i=1,2,3), a superposed dot indicates a time derivative, M_K is the lumped mass of node K, x is the vector of nodal Cartesian coordinates with respect to the global inertial reference frame, and $\ddot{x}$ is the vector of nodal accelerations with respect to the global inertial reference frame, F_s is the vector of internal structural forces, and F_a is the vector of externally applied forces, which include surface forces and body forces.

For each node representing a rigid body, a body-fixed material frame is defined. The origin of the body frame is located at the node that is also the body's center of mass. The mass of the body is concentrated at that node and the inertia of the body is given by the inertia tensor defined with respect to the body frame. The orientation of the body-frame is given by $R_K^{t_o}$ which is the rotation matrix relative to the global inertial frame at time t_0. The rotational equations of motions are written for each node with respect to its' body-fixed material frames as:

$$I_{Kij}\ddot{\theta}^t_{Kj} = T_{s}{}^t_{Ki} + T_{a}{}^t_{Ki} - \left(\dot{\theta}^t_{Ki} \times (I_{Kij}\dot{\theta}^t_{Kj})\right)_{Ki} \tag{2}$$

where I_K is the inertia tensor of rigid body K, $\ddot{\theta}_{Kj}$ and $\dot{\theta}_{Kj}$ are the angular acceleration and velocity vectors' components for rigid body K relative to its material frame in direction j (j=1,2,3), Ts_{Ki} are the components of the vector of internal torque at node K in direction i, and Ta_{Ki} are the components of the vector of applied torque. The summation convention is used only for the lower case indices i and j. Since, the rigid body rotational equations of motion are written in a body (material) frame, thus, the inertia tensor I_K is constant.

Unclassified: Distribution Statement A. Appropriate for public release; distribution is unlimited.

The trapezoidal rule is used as the time integration formula for solving equation (1) for the global nodal positions x:

$$\dot{x}_{Kj}^{t} = \dot{x}_{Kj}^{t-\Delta t} + 0.5\,\Delta t\,(\ddot{x}_{Kj}^{t} + \ddot{x}_{Kj}^{t-\Delta t}) \tag{3a}$$

$$x_{Kj}^{t} = x_{Kj}^{t-\Delta t} + 0.5\,\Delta t\,(\dot{x}_{Kj}^{t} + \dot{x}_{Kj}^{t-\Delta t}) \tag{3b}$$

where Δt is the time step. The trapezoidal rule is also used as the time integration formula for the nodal rotation increments:

$$\dot{\theta}_{Kj}^{t} = \dot{\theta}_{Kj}^{t-\Delta t} + 0.5\,\Delta t\,(\ddot{\theta}_{Kj}^{t} + \ddot{\theta}_{Kj}^{t-\Delta t}) \tag{4a}$$

$$\Delta\theta_{Kj}^{t} = 0.5\,\Delta t\,(\dot{\theta}_{Kj}^{t} + \dot{\theta}_{Kj}^{t-\Delta t}) \tag{4b}$$

where $\Delta\theta_{Kj}$ are the incremental rotation angles around the three body axes for body K. Thus, the rotational equations of motion are integrated to yield the incremental rotation angles. The rotation matrix of body K (R_K) is updated using the rotation matrix corresponding to the incremental rotation angles:

$$R_K^{t} = R_K^{t-\Delta t}\, R(\Delta\theta_{Ki}^{t}) \tag{5}$$

where $R(\Delta\theta_{Ki}^{t})$ is the rotation matrix corresponding to the incremental rotation angles from equation (4b).

The explicit solution procedure used for solving equations (1-5) along with constraint equations is presented in Section 7. The constraint equations are generally algebraic equations, which describe the position or velocity of some of the nodes. They include:

- Contact/impact constraints (Section 5):

$$f(\{x\}) \geq 0 \tag{6}$$

- Joint constraints (Section 6):

$$f(\{x\}) = 0 \tag{7}$$

- Prescribed motion constraints:

$$f(\{x\}, t) = 0 \tag{8}$$

3. Finite Elements

3.1 Truss/Spring Element

The truss element connects two nodes. The internal force in a truss element is given by:

$$F = \frac{EA}{l_0}(l - l_0) + \frac{CA}{l_0}\dot{l} \tag{9}$$

where E is the Young's modulus, C is the damping modulus, A is the cross-sectional effective area, l is the current length of the truss, l_0 is the un-stretched length of the truss.

3.2 Torsional-Spring Thin Spatial Beam Element

The torsional-spring beam element developed in [8] is used for modeling thin beams. The element has 3 point mass type nodes (nodes which have only translational DOFs). A beam element is shown in figure 2a The beam element connects the point p_1 (mid-point of $\overline{12}$) to point p_2 (mid-point of $\overline{23}$). The slope of the beam at p_1 is tangent to $\overline{12}$ and the slope of the beam at p_2 is tangent to $\overline{23}$. The beam element consists of two truss sub-elements ($\overline{p_1 2}$ and $\overline{2p_2}$) and a torsional-spring bending sub-element ($p_1\hat{2}p_2$). The internal force in a sub-truss element is given by equation (9). The internal moment in the bending sub-element is given by:

$$M = \frac{EI}{L_0}\Delta\alpha + \frac{CI}{L_0}\dot{\alpha} \tag{10}$$

where I is the cross-sectional effective moment of inertia, L_0 is the total un-stretched length of the bending element which is equal to the length of $\overline{p_1 2}$ plus $\overline{2p_2}$, and $\Delta\alpha$ is the change in angle between $\overline{p_1 2}$ and $\overline{2p_2}$ from the unstressed configuration. Figure 2b shows how a beam is discretized using the 3-noded beam element. This thin beam element does not have a torsional response along the axis of the beam. In addition, it assumes that the bending moments of inertia of the cross-section around two perpendicular cross-section axes are the same.

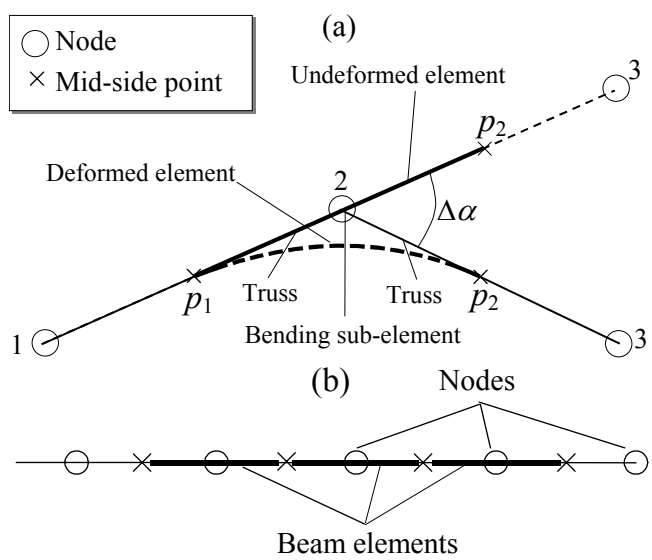

Figure 2. (a) 3-noded beam element; (b) finite element discretization of a beam using the 3-noded beam element.

Unclassified: Distribution Statement A. Appropriate for public release; distribution is unlimited.

3.3 Lumped Parameters Thick Spatial Beam Element

A lumped parameter spatial beam element is used to model thick beams. The element has two rigid body type nodes. Therefore, each node has 3 translational DOFs and the rotation matrix is used to measure the spatial rotation of the node. The beam element local *X*-axis is in the direction of the line connecting the two nodes. The *Y* and *Z* axes are normal to the *X*-axis and to each other. They are defined as an average of the local *Y* and *Z* axes of the two nodes. The element models each response component independently using simpler elements (figure 3):

- Axial response is modeled using a zero-length linear spring-damper truss element at the center point between the two nodes. The internal force along the *X*-axis for the truss element is given by:

$$F_x = \frac{EA}{l_0} d_x + \frac{CA}{l_0} \dot{d}_x \tag{11}$$

  where E is the Young's modulus, C is the damping modulus, A is the cross-sectional area, l_0 is the unstretched length of the beam and d_x is the deflection between two nodes along the beam's *X*-axis.

- Shear response is modeled using two zero-length linear spring-damper elements located at the center point between the two nodes. One element produces a reaction force along the element *Y*-axis and the other element produces a reaction force along the element *Z*-axis. The internal forces for the *Y*-truss element along the *Y*-axis and for the *Z*-truss element along the *Z*-axis are given by:

$$F_y = \mathrm{K}_y \left(\frac{GA}{l_0} d_y + \frac{CA}{l_0} \dot{d}_y \right) \tag{12a}$$

$$F_z = \mathrm{K}_z \left(\frac{GA}{l_0} d_z + \frac{CA}{l_0} \dot{d}_z \right) \tag{12b}$$

  where G is the shear modulus, K_y and K_z are the cross-section shear factors, and d_y and d_z are the deflections between two nodes along the beam's *Y*-axis and *Z*-axis, respectively.

- Bending response is modeled using two torsional spring-damper elements located at the center point between the two nodes. One element produces the bending response around the *Y*-axis and the other element produces the bending response around the *Z*-axis. The internal moments for the *Y* torsional element and for the *Z* torsional element are given by:

$$M_y = \frac{EI_{yy}}{l_0} \alpha_y + \frac{CI_{yy}}{l_0} \dot{\alpha}_y \tag{13a}$$

$$M_z = \frac{EI_{zz}}{l_0} \alpha_z + \frac{CI_{zz}}{l_0} \dot{\alpha}_z \tag{13b}$$

  where I_{yy} *and* I_{zz} are the second moments of inertia of the cross-section around the *Y* and *Z* axes, respectively, α_y and α_z are the change in angles between two nodes around the beam's *Y*-axis and *Z*-axis, respectively.

- Torsional response is modeled using a torsional spring-damper element located at the center point between the two nodes. The element produces the torsional response around the *X*-axis. The internal moments for the *X* torsional element is given by:

$$M_x = \frac{EJ}{l_0} \alpha_x + \frac{CJ}{l_0} \dot{\alpha}_x \tag{14}$$

  where J is the torsional moment of inertia of the cross-section, α_x is the change in angle between two nodes along the beam's *X*--axis.

The deflections d_x, d_y and d_z can be obtained as follows. The center point the element for each of the element nodes found (X_{C1_i}, X_{C2_i}, i = 1,2,3). Then, the vector connecting the two points is found:

$$U_{12_i} = X_{C2_i} - X_{C1_i} \tag{15}$$

The dot product vector $\vec{U}_{12}$ with the *X*-axis, *Y*-axis and *Z*-axis vectors of the beam give d_x, d_y and d_z, respectively. The angle changes α_x, α_y and α_z can be found using the nodes rotation matrices.

The main features of the lumped parameters beam element are:

- It can model spatial beams including bending along the two transverse cross-section directions and torsion.
- Shear deformation is modeled.
- Since the beam is modeled using nodes having both translational and rotational DOFs (therefore, they can be thought of as rigid bodies), therefore, detailed 3D contact surfaces for the beam can be used. This allows the use of this beam element to model the detailed geometry of track segments.

Unclassified: Distribution Statement A. Appropriate for public release; distribution is unlimited.

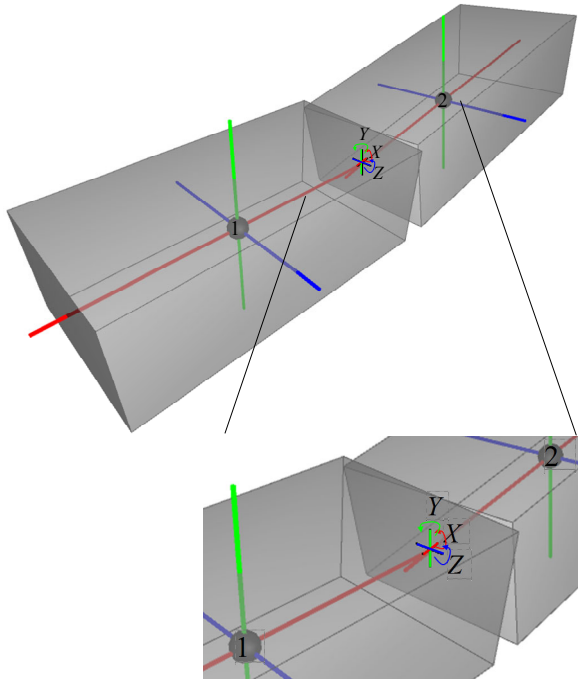

Figure 3. Spatial lumped parameters 2-node beam element. Each node is modeled as a rigid body. The *X*, *Y*, *Z* local axes of each node are shown red, green and blue, respectively. The element consists of 3 truss elements (for modeling the axial and shear response) and 3 torsional spring elements (for modeling the bending and torsion response) located at the center point of the element.

3.4 Natural-Modes Brick Element

The 8-nodes natural-modes brick element developed in [9, 10] is strategically designed to model all the deformation and rigid body modes (figure 4) of a brick element while avoiding locking and spurious modes. All the element nodes are point mass type nodes with only translational DOFs.

Two types of sub-elements are used to model the brick: two-node truss element and four-node surface shear element. Twelve truss elements along the twelve edges of the element are used to model the membrane and bending modes of the element. Six surface shear elements are introduced at each of the six element surfaces to model the shear and warping modes of the element (figure 5). The derivations of the stiffness characteristics and structural forces generated by the truss and the surface shear elements are given in . The brick element with the following characteristics:

- The deformation element modes, including, membrane, bending, shear, and warping are accurately modeled. Thus the element does not have any spurious modes.
- The shear stresses are evaluated as the average stresses over each of the element faces, thus the element does not exhibit shear locking.
- All element structural forces are aligned with the element edges, thus the element does not exhibit membrane or membrane-warping locking.

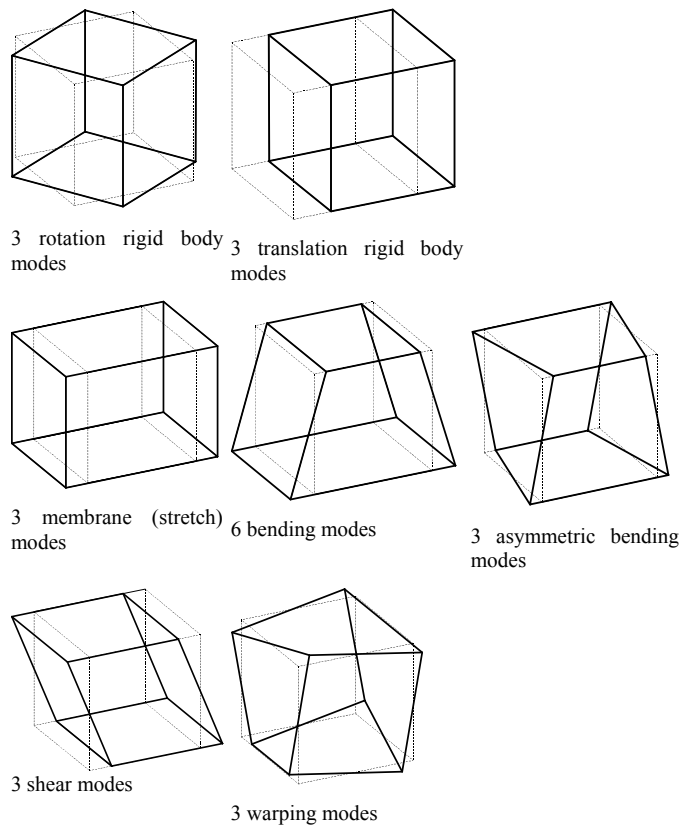

Figure 4. 24 rigid body and deformation modes of a spatial 8-node brick element.

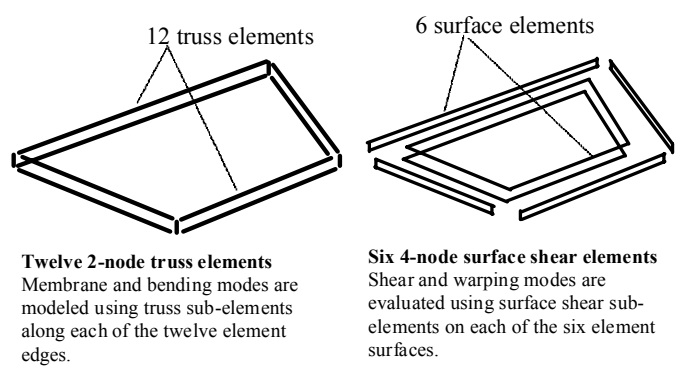

Figure 5. Sub-elements of the 8-node lumped-parameters brick element.

4. CONTACT MODEL

The penalty technique is used to impose the normal contact constraints between finite element nodes or points on a rigid body and finite element surfaces or quadrilateral surfaces of

Unclassified: Distribution Statement A. Appropriate for public release; distribution is unlimited.

rigid bodies [5, 6]. The first step is to find the position and velocity of the contact nodes and points. For finite element nodes the global position x_{Gp} and velocity $\dot{x}_{Gp}$ of a contact node relative to the global inertial frame are readily available:

$$x_{Gp_i} = x_{Ki} \tag{16a}$$

$$\dot{x}_{Gp_i} = \dot{x}_{Ki} \tag{16b}$$

where x_{Ki} and $\dot{x}_{Ki}$ are the position and velocity vectors of contact node *K*. For rigid bodies the global position x_{Gp} and velocity $\dot{x}_{Gp}$ of a contact point are given by:

$$x_{Gp_i} = X_{BF_i} + R_{BF_{ij}}\, x_{Lp_j} \tag{17a}$$

$$\dot{x}_{Gp_i} = \dot{X}_{BF_i} + R_{BF_{ij}}\,(W_{BF} \times x_{Lp})_j \tag{17b}$$

where X_{BF} and $\dot{X}_{BF}$ are the global position and velocity vectors of the rigid body's frame, R_{BF} is the rotation matrix of the rigid body relative to the global reference frame, W_{BF} is the rigid body's angular velocity vector relative to its local frame, and x_{Lp} is the position of the contact point relative to the rigid body's frame.

The frictional contact force F_c at each contact point/node (sum of the normal contact and tangential friction forces) is transferred as a force and a moment to the center of the rigid body. The negative of this force is transferred to the contact surface element by distributing it to the nodes forming the surface using the element shape function:

$$F_{ki} = -N_k\, F_{c_i} \tag{18}$$

where N_k are the surface element shape functions at the contact point and F_{ki} are the contact forces on node k of the surface element. In case the contact body is a rigid body, then this force can also be transferred to the center of the contacting rigid body as a force and moment:

$$F_i = -F_{c_i} \tag{19a}$$

$$M_i = -(x_{Lp_i} \times R_{BF_{ji}} F_{c_i}) \tag{19b}$$

$$x_{Lp_j} = R_{BF_{ji}}(x_{Gp_i} - X_{BF_i}) \tag{20}$$

where F_i is the contact force at the CG of the contact rigid body (center of the body frame), M_i in the contact moment on the contact rigid body, x_{Lcp} is the position of the contact point relative to the rigid body's frame and x_{Gcp} is the position of the contact point relative to the global reference frame. Thus, the contact algorithm supports contact flexible-flexible, rigid-rigid and rigid-flexible body contact.

4.1 Penalty Normal Contact Model

The penalty technique is used for imposing the constraints in which a normal reaction force (F_{normal}) is generated when a node penetrates in a contact body whose magnitude is proportional to the penetration distance. In the present formulation, the force is given by [5, 6]:

$$F_{normal} = A\,k_p\,d + A\begin{cases} c_p\,\dot{d} & \dot{d} \geq 0 \\ s_p\,c_p\,\dot{d} & \dot{d} < 0 \end{cases} \tag{21}$$

$$\dot{d} = v_{n_i}\, n_i \tag{22}$$

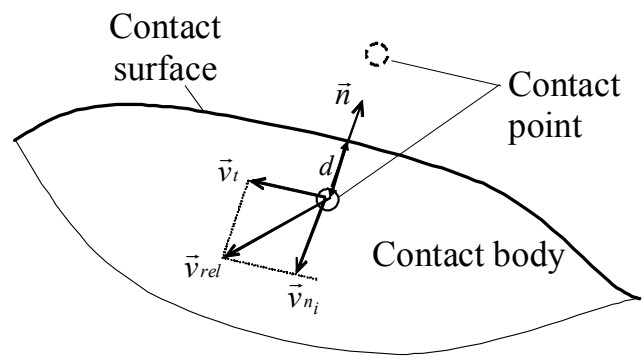

Figure 6. Contact surface and contact node.

where A is the area of the rectangle associated with the contact point, k_p and c_p are the penalty stiffness and damping coefficient per unit area; d is the closest distance between the node and the contact surface (figure 6); $\dot{d}$ is the signed time rate of change of d; s_p is a separation damping factor between 0 and 1 which determines the amount of sticking between the contact node and the contact surface at the node (leaving the body); $\vec{n}$ is the normal to the surface and $\vec{v}_{n_i}$ is the velocity vector in the direction of $\vec{n}$. The normal contact force vector is given by:

$$F_{n_i} = n_i\, F_{normal} \tag{23}$$

The total force on the node generated due to the frictional contact between the point and surface is given by:

$$F_{point_i} = F_{t_i} + F_{n_i} \tag{24}$$

4.2 Asperity Friction Model

An asperity-spring friction model is used to model joint and contact friction [20] in which friction is modeled using a piece-wise linear velocity-dependent approximate Coulomb friction element in parallel with a variable anchor point spring. The model approximates asperity friction where friction forces between two rough surfaces in contact arise due to the interaction of the surface asperities. F_{t_i} is the

Unclassified: Distribution Statement A. Appropriate for public release; distribution is unlimited.

tangential friction contact force vector transmitted to the contact body at the contact point. It is given by:

$$F_{t_i} = F_{tangent}\ t_i \tag{25}$$

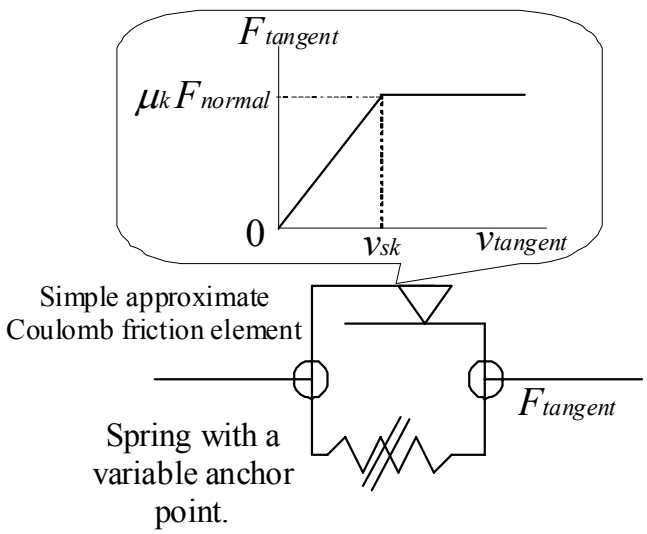

Figure 7. Asperity spring friction model.

The asperity friction model is used along with the normal force to calculate the tangential friction force ($F_{tangent}$) [7]. When two surfaces are in static (stick) contact, the surface asperities act like tangential springs. When a tangential force is applied, the springs elastically deform and pull the surfaces to their original position. If the tangential force is large enough, the surface asperities yield (i.e. the springs break) allowing sliding to occur between the two surfaces. The breakaway force is proportional to the normal contact pressure. In addition, when the two surfaces are sliding past each other, the asperities provide resistance to the motion that is a function of the sliding velocity and acceleration, and the normal contact pressure. Figure 7 shows a schematic diagram of the asperity friction model. It is composed of a simple piece-wise linear velocity-dependent approximate Coulomb friction element (that only includes two linear segments) in parallel with a variable anchor point spring.

4.3 Contact Search

Contact detection is performed between contact points on a "master contact surface" and a polygonal surface called the "slave contact surface". The contact points of the master contact surface can either be point mass nodes or points on a contact surface of a rigid body type node. The slave contact surface can be a polygonal surface connecting point mass type nodes or a polygonal surface on a rigid body type node. Contact between the contact points of the master surface and the polygons of the slave surface is detected using a binary tree contact search algorithm which allows fast contact search. At the initialization of the algorithm the following steps are performed:

- Each slave polygonal contact surface is divided into 2 blocks of polygons. The bounding box for each block of polygons is found. Then each of those blocks of polygons is divided into 2 blocks and again the bounding boxes for those blocks are found. This recursive division continues until there is only one polygon in a box.
- For each master contact surface the contact points are divided into 2 blocks. The bounding sphere for each block of points is found. Then, each of those blocks of points is divided into 2 blocks and again the bounding spheres for those blocks are found. This recursive division continues until there is only one point (with a bounding sphere of radius 0).

During the solution the following steps are performed. For each master contact sphere, the radius of the contact sphere is added to the size of the bounding box, and then we check if the center point of the sphere is inside a bounding box. If the center of the contact sphere is not inside any bounding box, then all the points inside that sphere are not in contact with the surface. If the center of the contact sphere is inside a bounding box then the two sub-bounding boxes are checked to determine if the point is inside either one. If it is, then the sub-contact spheres are checked. If a contact point is found to be inside the lowest level bounding box, then a more computationally intensive contact algorithm between a point and a polygon is used to determine the depth of contact and the local position of the contact point on the polygon.

This search algorithm has a theoretical average computational cost of $\log(m) \times \log(n)$, where m is the number of points of the master surface and n is the number of polygons of the slave surface. It allows detecting contact between surfaces containing millions of polygons and contact points in near real-time.

5. JOINT CONSTRAINTS

Each rigid body can have a number of connection points. A connection point is a point on the body where joints can be located. A connection point does not add additional DOFs to the system .The connection point can be:

- A point mass type node.
- A point on a rigid body.
- An arbitrary point inside a finite element.

5.1 Connection point location

If the connection point is a node then equations (16a) and (16b) are used to find the global position x_{Gp} and velocity

Unclassified: Distribution Statement A. Appropriate for public release; distribution is unlimited.

$\dot{x}_{Gp}$ of the connection point. If the connection point is a fixed point on rigid body B then equations (17a) and (17b) are used to find the global position and velocity of the connection point. If the connection point is a point inside a finite element, then x_{Gp} and velocity $\dot{x}_{Gp}$ are given by:

$$x_{Gp}{}_i^t = N_J(\xi_l)\ x_{Ji}^t \tag{26}$$

$$\dot{x}_{Gp}{}_i^t = N_J(\xi_l)\ \dot{x}_{Ji}^t \tag{27}$$

where J is the local node number of the element, $N_J(\xi_l)$ are the interpolation functions of the element, ξ_l are the natural element coordinates of the fixed point and x_{Ji}^t is the position vector of local node J of the element relative to the global reference frame.

5.2 Spherical joint constraint force

A joint is defined by defining the relation between connection points. For example, a spherical joint between two connection points is defined as:

$$x_{c1}{}_i^t = x_{c2}{}_i^t \tag{28}$$

where $x_{c1}{}_i^t$ is the position vector of the first point and $x_{c2}{}_i^t$ is the position vector of the second point. This constraint is imposed using the penalty technique as:

$$F_c = k_p |v| + c_p\ v_i \dot{v}_i \tag{29}$$

$$v_i = x_{c1}{}_i^t - x_{c2}{}_i^t \tag{30}$$

$$\dot{v}_i = \dot{x}_{c1}{}_i^t - \dot{x}_{c2}{}_i^t \tag{31}$$

$$F_{c_i} = F_c\, v_i \tag{32}$$

where F_{c_i} is the penalty reaction force on the connection point, k_p is the penalty spring stiffness, and c_p is the penalty damping. The constraint force is applied on the two connection points in opposite directions. Depending on the type of connection point the constraint force is applied as follows. If the connection point is a point on a rigid body, then it is transferred to the node at the center of the body as a force and a moment using equations (14a) and (14b). If the connection point is a node, then the constraint force is applied directly to the node:

$$F_{Ki}^t = F_{c_i}^t \tag{33}$$

If the connection point is a point inside a finite element, then it is applied to the nodes of the element using:

$$F_{Ji}^t = N_J(\xi_l)\ F_{c_i}^t \tag{34}$$

where J is the local node number of the element, F_{Ji}^t is the force on local node J of the element relative to the global reference frame.

Using equations (16, 17, and 26-34), the following types pin joints can be modeled:

- Spherical -joint between two rigid bodies.
- Spherical-joint between a rigid body and a finite element point.
- Spherical-joint between a rigid body and a point particle type node.
- Spherical-joint between two element points.
- Spherical-joint between an element point and a point particle type node.
- Spherical-joint between two nodes.

The constraint forces are applied to the connection point node(s) by assembling them into the global structural forces F_s in equation (1). Also, the constraint moments are applied to the nodes by assembling them into the global structural torques T_s in equation (2).

Revolute joints can be modeled by placing two spherical joints along a line. Other types of joints such as prismatic, cylindrical, universal and planar joints can also be modeled by writing the constraint equation, then writing the corresponding penalty forces and moments on the connection points.

6. EXPLICIT SOLUTION PROCEDURE

The solution fields for modeling multibody systems are defined at the model nodes. Note that a rigid body modeled as one finite element node. These solutions fields are:

- Translational positions.
- Translational velocities.
- Translational accelerations.
- Rotation matrices.
- Rotational velocities.
- Rotational accelerations.

The explicit time integration solution procedure predicts the time evolution of the above response quantities. An advantage of explicit solution procedures is that they are "embarrassingly" parallel. The procedure described below achieves near linear speed-up with the number of processors on shared memory parallel computers. The procedure is implemented in a multibody dynamics finite element code and is outlined below:

1- Prepare the run:

a. Set the initial conditions for the solution fields identified above.

Unclassified: Distribution Statement A. Appropriate for public release; distribution is unlimited.

b. Create a list of all the finite elements (Those also include joints and master contact surfaces which are considered elements).
c. Create a list of elements that will run on each processor. This is done using an algorithm which tries to make the computational cost on each processor equal.
d. Create a list of all the prescribed motion constraints.
e. Calculate the solid masses for each finite element node by looping through the list of finite elements. Note that the masses are fixed in time.
f. Loop over all the elements and find the minimum time step for the explicit solution procedure.

2- Loop over the solution time and increment the time by Δt each step while doing the following:

a. Set the nodal values at the last time step to be equal to the current nodal values for all solution fields.
b. Do 2 iterations (a predictor iteration and a corrector iteration) of the following:
   i. Initialize the nodal forces and moments to zero.
   ii. Calculate the nodal forces and moments by looping through all the elements (and joints) while calculating and assembling the element nodal forces. This is the most computational intensive step. This step is done in parallel by running each list of elements identified in step 1.c on one processor.
   iii. Find the nodal values at the current time step using the semi-discrete equations of motion and the trapezoidal time integration rule (Eqs. 1-5).
   iv. Execute the prescribed motion constraints which set the nodal value(s) to prescribed values.
   v. Go to the beginning of step 2.

7. EXPERIMENTAL SETUP

The model is validated using a full-scale army tracked vehicle. The track was removed and the vehicle was placed on an n-post motion base simulator in the US army's Tank Automotive Research, Development and Engineering Center's (TARDEC) Simulation Laboratory (TSL) (see figures 1 and 8). The n-post motion simulator consists of linear hydraulic actuators each placed under one of the vehicle road wheels. The road-wheels are connected to the road arms using revolute joints. The vehicle suspension system consists of the road arms and torsion bars between the roads arms and chassis. The road arms are connected to the chassis using revolute joints. Each road arm is free to rotate between two hard suspension stops at 0 degrees (when the arm is horizontal) and about 60 degrees from the horizontal. Each actuator has one degree of freedom along the vertical direction and can be independently commanded to follow a certain vertical displacement time-history. Thus, the actuators can be controlled in such a way as to simulate vertical position time-histories of the wheels as the vehicle goes over a rough road that has bumps and potholes. Note that the motion simulator cannot simulate the inertial centrifugal inertia forces that arise due to the time-varying motion of the vehicle on the road.

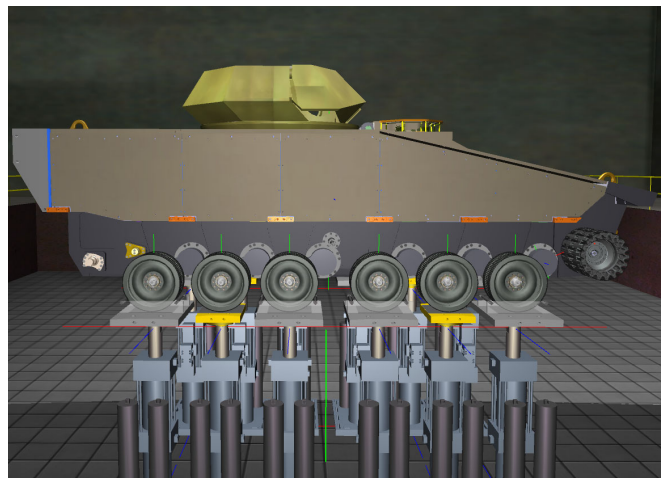

Figure 8. Snapshot of the computational model of the tracked vehicle on the n-post motion simulator.

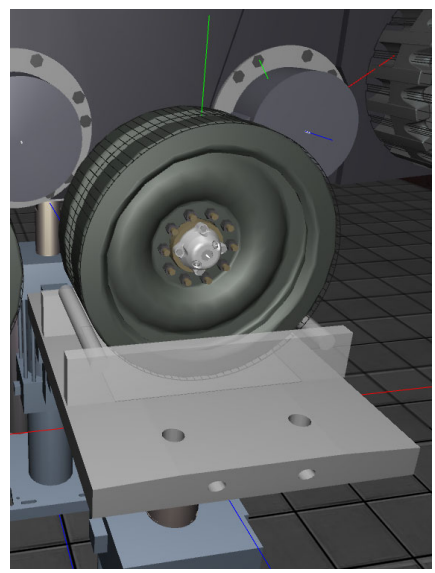

Figure 9. Dishpans with front and back cylindrical stops and side guard rails.

The vehicle in our experimental setup has 12 road wheels, 6 on each side. We number the wheels from front to back 1 through 6. Each hydraulic actuator is composed of a cylinder, piston and a dishpan on which the wheel rests. The dishpans for wheels 1, 3, 4 and 6 (colored silver) have front

Unclassified: Distribution Statement A. Appropriate for public release; distribution is unlimited.

and back horizontal cylindrical stops as well as side guard rails (figure 9). Those dishpans are used in order to ensure that the vehicle does not "slide off" the motion simulator. Flat dishpans are used for wheels 2 and 5 (figure 10). In addition, a strap harness was attached to the top of the vehicle during the experiments for safety reasons. The harness was loose so as not to interfere with the motion of the vehicle.

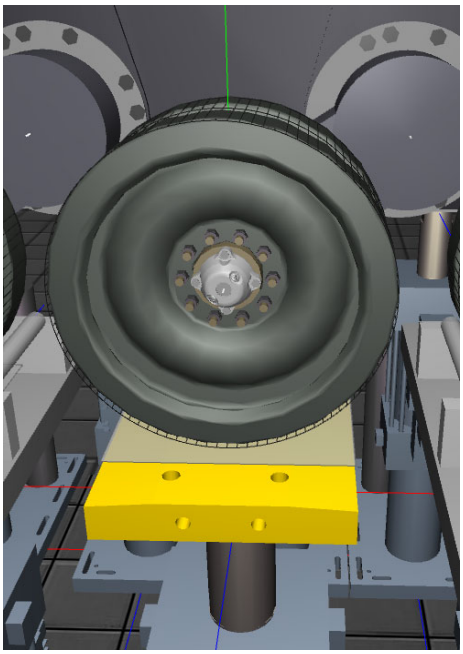

Figure 10. Flat dishpans.

The angles of the 12 roads arms are measured and sampled at a rate of 205 samples/sec. The experiment 12 road arms angles measurements are compared with the results predicted using the computational model. A camera mounted on the ground is used to record the motion of the vehicle. The camera is set to capture 30 frames/sec. The camera view is shown in figure 8.

The torsion bars at the road wheels were charged such that the road arms are initially half way between the two suspension stops (i.e. at about 30 degrees from the horizontal) when the vehicle is at rest under gravity and the track is off. Figure 11 shows the rotational stiffness (torque versus angle) of the torsion bar at each road wheel. The torsion bars rotational stiffness was experimentally obtained.

The matrix of excitations applied to the vehicle is shown in Table 1. Two main types of excitations are used: shake and pitch. In the shake excitation all the actuators are moving the same way (i.e. their motions are in phase). In the pitch excitation the front and rear actuators are 180° out of phase. The intermediate actuators are moved in such as way that at, at point in time, the line connecting the center of the front dishpan and center of the rear dishpan passes through the center of the intermediate dishpans. This way the vehicle is rotating around its pitch axis. The pitch and shake excitations simulate the vehicle going over bumps and potholes. For each motion type, harmonic excitations at amplitudes 40, 60 or 70 mm and frequencies from 0.6 to 1.5 Hz are applied to the vehicle. Each excitation is applied for about 15 sec with the initial 3 sec and the last 3 sec used to ramp up and down the excitation amplitude. Also, for each ramp motion type, a ramp excitation of 90 mm is applied to the vehicle, where the vehicle is raised 90 mm in 0.2 sec, then the actuators dwell for 5 sec, finally the vehicle is lowered 90 mm in 0.2 sec.

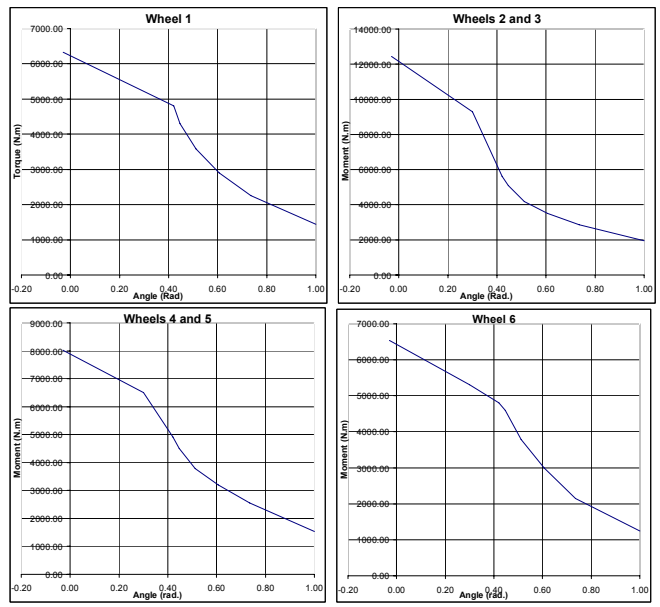

Figure 11. Experimetally measured rotational stiffness (torque versus angle) of the torsion bar at each road wheel.

Table 1. Matrix of the tracked vehicle experiments (38 experiments).

Excitation	Amplitude	Frequency (Hz)	Ramp Duration (sec)
Harmonic – Pitch	40 mm	0.6; 0.7; 0.8; 0.9;1.0; 1.1; 1.2; 1.3; 1.4	-
	60 mm	1.1; 1.2	-
	70 mm	0.6; 0.7; 0.8; 0.9;1.0	-
Harmonic – Shake	40 mm	0.6; 0.7; 0.8; 0.9; 1.0; 1.1; 1.2; 1.3; 1.4; 1.5	-
	70 mm	0.6; 0.7; 0.8; 0.9; 1.0; 1.1; 1.2; 1.3; 1.4; 1.5	-
Ramp – Pitch	90 mm	-	0.2
Ramp – Shake	90 mm	-	0.2

Unclassified: Distribution Statement A. Appropriate for public release; distribution is unlimited.

8. VALIDATION STUDY

The experiments in Table 1 were simulated using the present model. First the experiments were used to find an average damping moment versus angular velocity for the suspension system's torsion bars (figure 12). This average damping moment versus angular velocity curve was used for all the torsion bars. The damping moment versus angular velocity typically depends on the oil charge of the torsion bar. Note that the curve is nonlinear. For very small angular velocities, the tension bar produces a large amount of damping. For larger values of angular velocity, the damping moment is nearly linear with angular velocity, and gradually deviates from linearity and becomes stiffer for very large angular velocities. Also, from the experiments we found that there is small friction moment in the tension bars of about 5 N.m. Note that the present model accounts for non-linear stiffness, damping and friction of the suspension system. Also, the model allows the wheels to leave the dishpans.

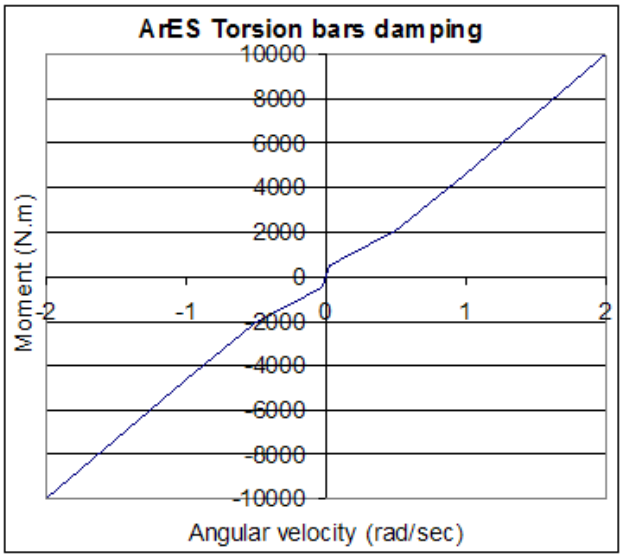

Figure 12. Damping moment versus angular velocity for the torsion bars.

The graphs in Figures 13-20 show the results of 4 representative runs from the set of 38 runs in the test matrix shown in Table 1. Those figures show comparisons of the road arm angles between the experiment and the DIS simulation. The average difference in magnitude between the experiment and simulation is about 15%. The average response difference between the right and left sides of the vehicle was also about 15%. The main sources of error between the experiments and simulation in order of importance are:

- At the higher frequency shake excitations (1.4, 1.5 Hz) and pitch excitations (1.0, 1.1 and 1.2 Hz), the amplitude of motion of the road arms exceeded ±6°. At those amplitudes, the wheels where bumping and "climbing over" the dishpans cylindrical stops. The experimental results for those runs cannot be accurately modeled because the position of a wheel relative to the dishpans stops is not known and varies between runs. For those excitations the difference between the experiment and simulation was on the average about 30% with a maximum difference of about 50%. Also, note that the range of motion of a road arm is about ±29°, but the highest motion amplitude that we tested was about ±10 degrees. We could not excite the vehicle beyond ±10 degrees road arm deflections for safety reasons since the wheels started bumping and going over the stops at ±6°.
- Asymmetry of the stiffness and damping between the two sides of the vehicle. The difference between the response at the two sides of the vehicle was on average about 8%.
- Presence of the strap harness.

9. TYPICAL SIMULATIONS

The present model can be used to predict the dynamic response of tracked vehicle. This includes predicting the following:

- Stability of the vehicle while moving at a certain speed over a rough terrain or while steering.
- Maximum positive or negative obstacles that the vehicle can overcome. This includes initial speed and engine torque required to overcome the obstacle.
- Internal forces in the various components of the vehicle including the track while going over various terrains and obstacles. Those forces can then be applied to finer finite element models of the components for detailed stress analysis. The predicted stresses can be used to determine the whether the component will fail under the loads as well as the fatigue life of the component.
- Vehicle energy and power requirements for going at a prescribed speed over a known course.

Further experimental tests are needed to validate and tune the model parameters to accurately predict the above response quantities. Those experiments should include actual road tests using an instrumented tracked vehicle.

Unclassified: Distribution Statement A. Appropriate for public release; distribution is unlimited.

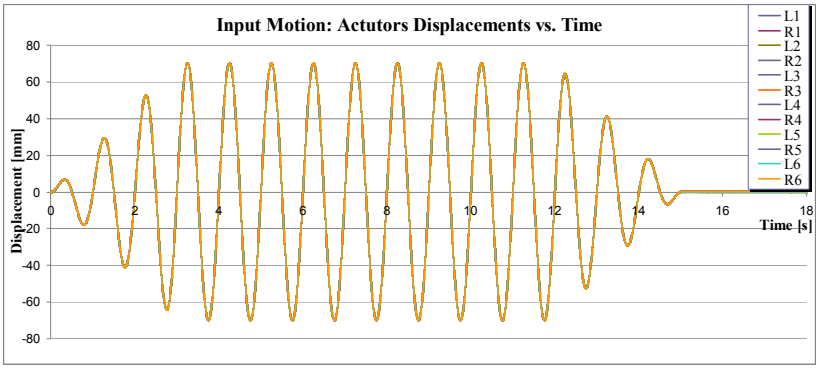

Figure 13. Input motion: harmonic shake 1.0 Hz 70 mm.

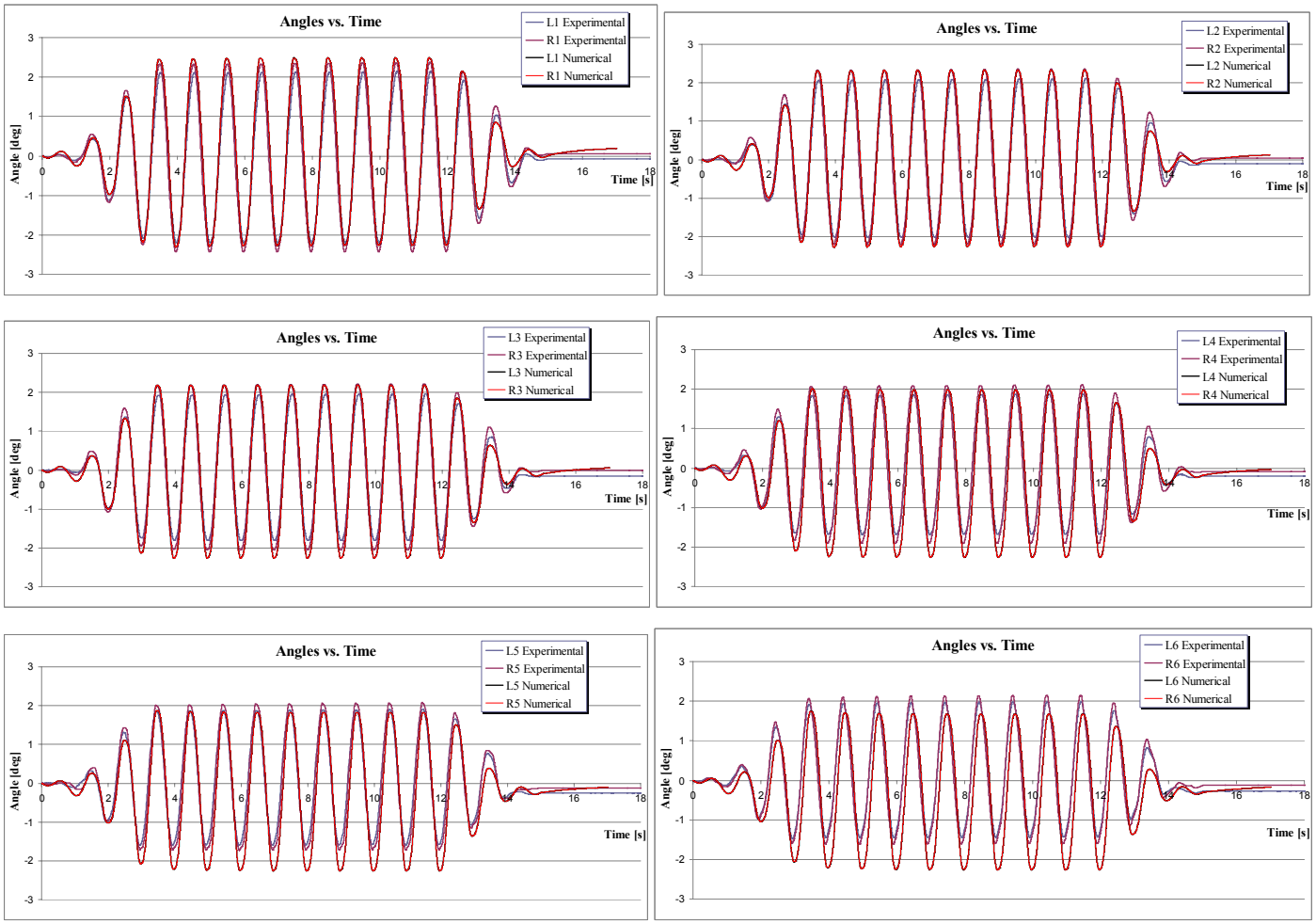

Figure 14. Experiment and simulation angles of the road arms versus time for input motion: harmonic shake 1.0 Hz 70 mm.

Unclassified: Distribution Statement A. Appropriate for public release; distribution is unlimited.

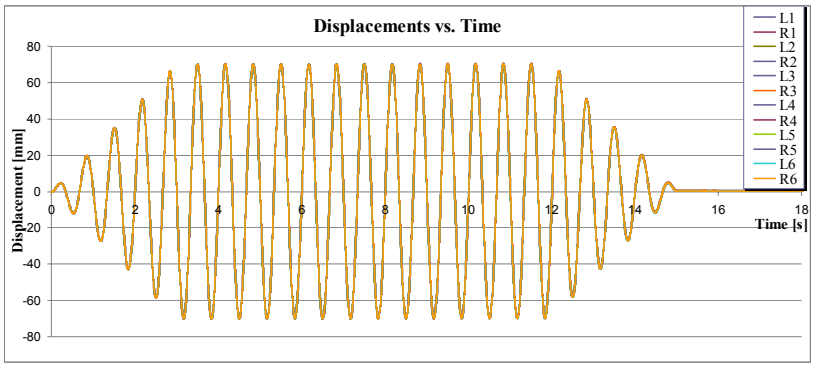

Figure 15. Input motion: harmonic shake 1.5 Hz 70 mm.

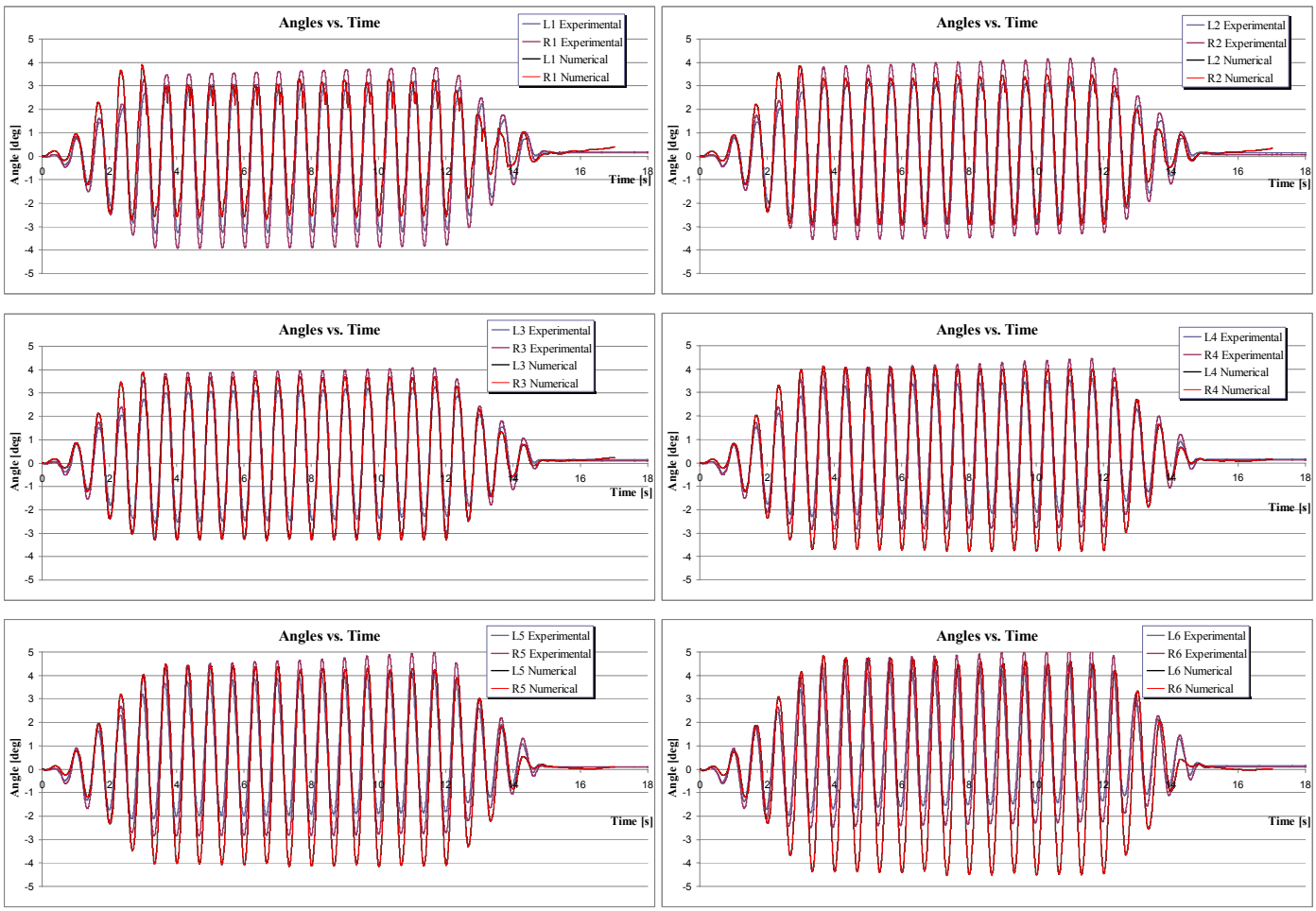

Figure 16. Experiment and simulation angles of the road arms versus time for input motion: harmonic shake 1.5 Hz 70 mm.

Unclassified: Distribution Statement A. Appropriate for public release; distribution is unlimited.

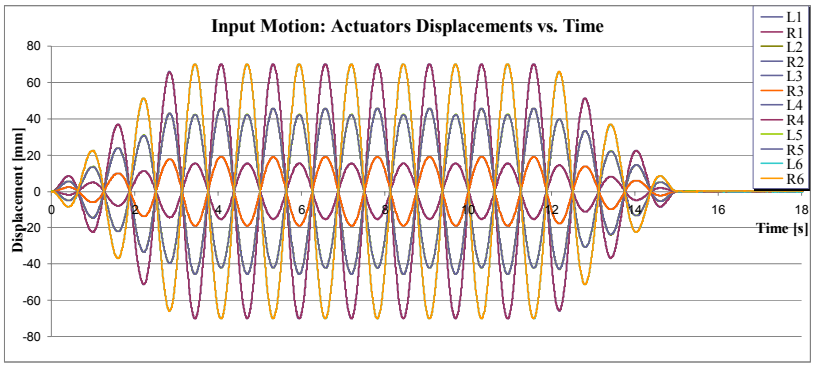

Figure 17. Input motion: harmonic pitch 0.8 Hz 70 mm.

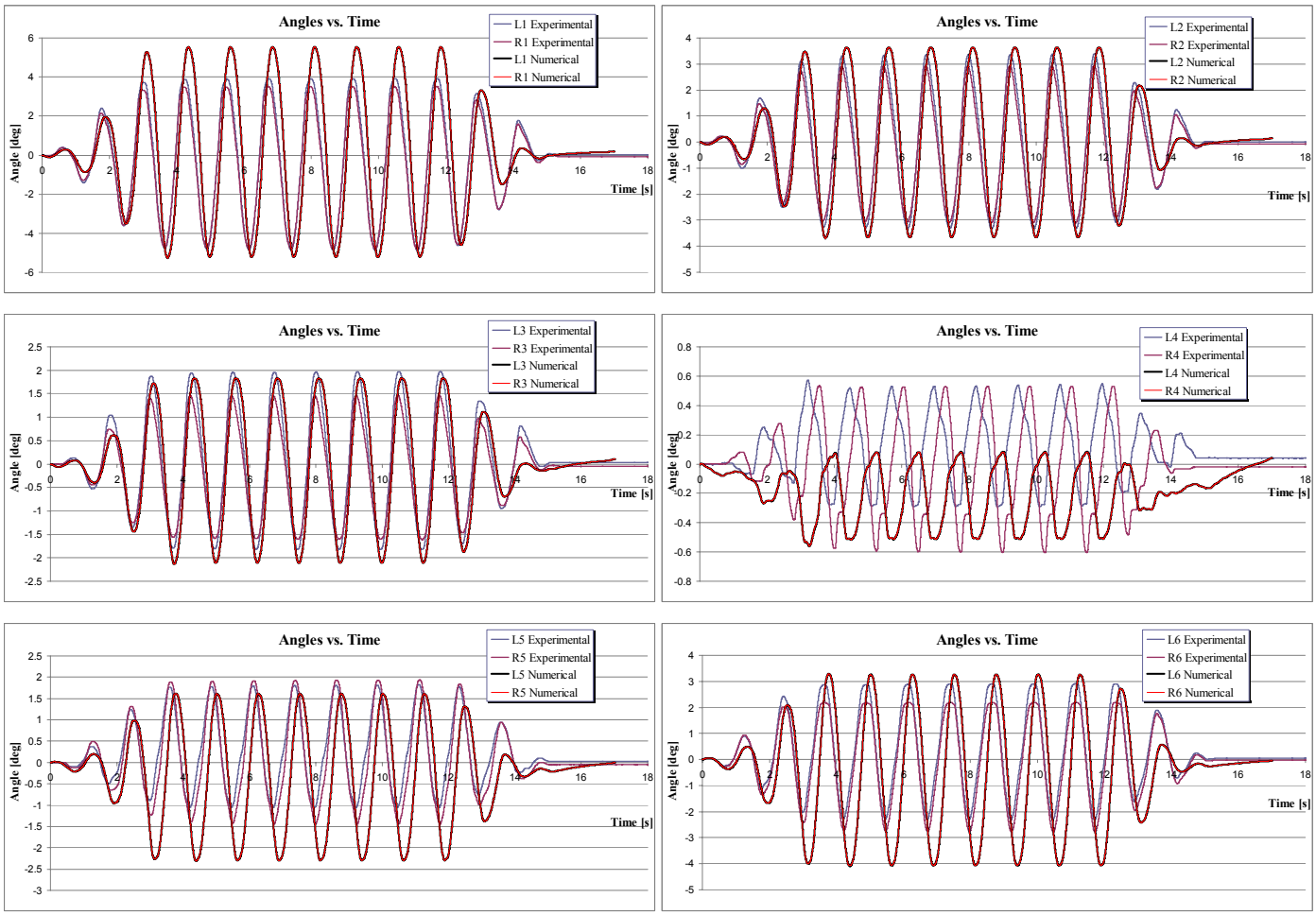

Figure 18. Experiment and simulation angles of the road arms versus time for input motion: harmonic pitch 0.8 Hz 70 mm.

Unclassified: Distribution Statement A. Appropriate for public release; distribution is unlimited.

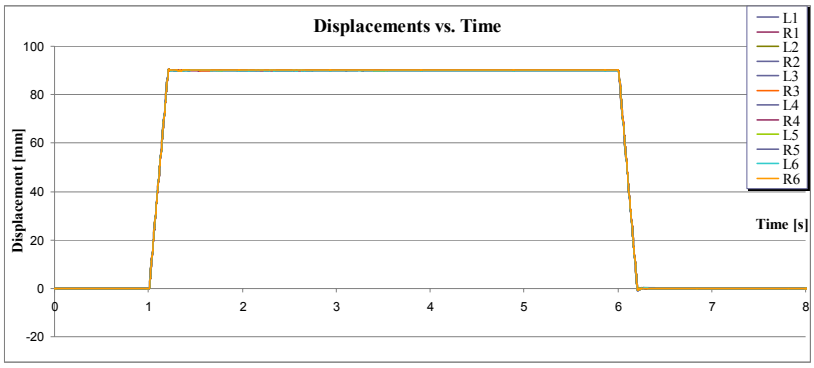

Figure 19. Input motion: ramp shake 90 mm.

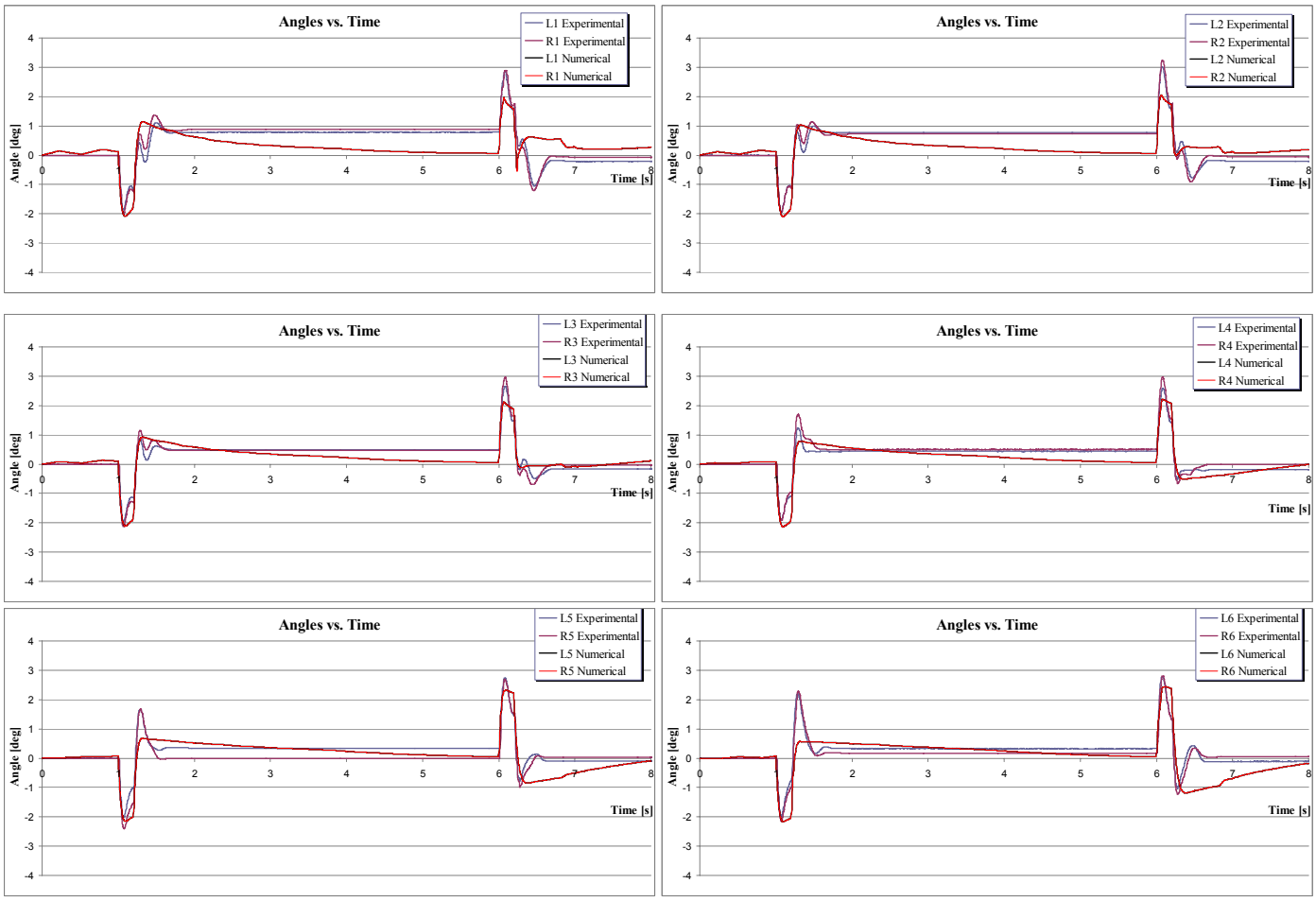

Figure 20. Experiment and simulation angles of the road arms versus time for input motion: ramp shake 90 mm.

Unclassified: Distribution Statement A. Appropriate for public release; distribution is unlimited.

(a)

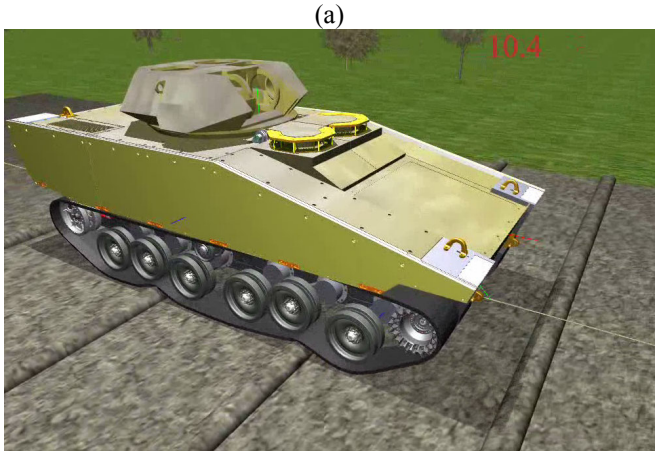

(b)

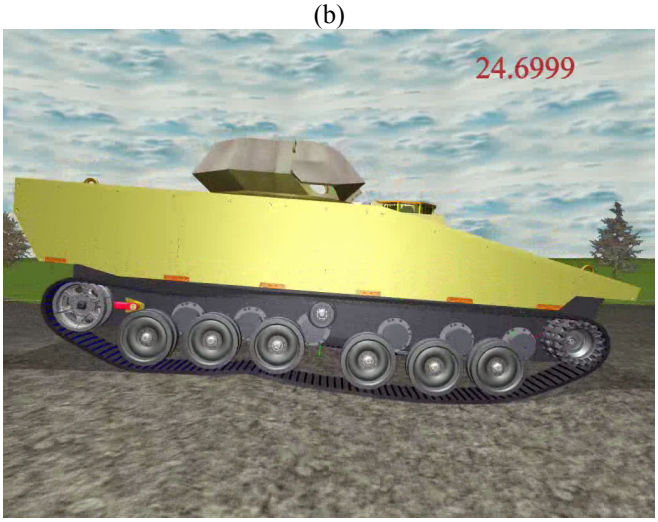

Figure 21. Snapshots of the motion of the tracked vehicle with a continuous belt track. The track is modeled using brick elements for modeling the belt rubber and thin beam elements for modeling the reinforcements. (a) vehicle going over.semi-circular bumps; (b) vehicle going over a rough course.

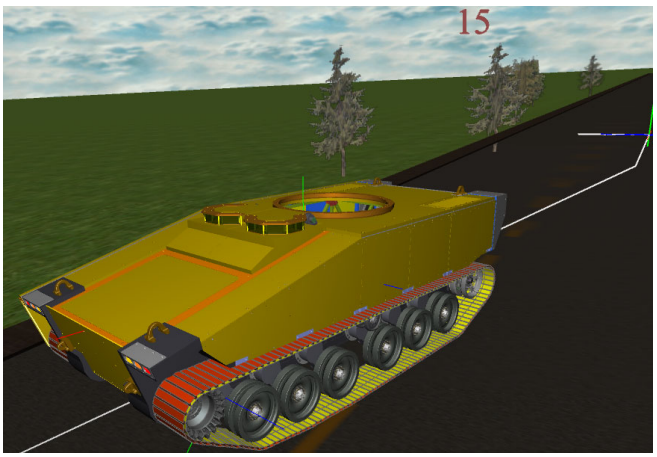

Figure 22. Snapshot of the motion of the tracked vehicle with a continuous belt track modeled using thick beam elements.

Finite element models of a typical tracked vehicle, with a continuous belt-type track, are shown in Figures 21 and 22. In those models the chassis, road arms, road wheels, idlers and sprockets are modeled using rigid bodies. The suspension rotary spring-dampers are modeled as torsional springs. Rotary actuators along with control laws are used to model the engine and steering system of the vehicle. In Figure 21 the track is modeled using brick elements for the rubber matrix and thin beam for the reinforcements. In Figure 22 the track is modeled using the thick beam elements presented in Section 3.3. Figures 21a shows a snapshot of the tracked vehicle going over semi-circular bumps. Figure 21b shows a snap shot of the tracked vehicle going over a rough course. Figure 22 shows a snapshot of the tracked vehicle undergoing a lane-change.

10. CONCLUDING REMARKS

A finite element model for predicting the fully coupled dynamic response of flexible multibody systems for tracked vehicles was presented. The model has the following characteristics:

- Parallel explicit time-integration solver.
- Algorithm for accurate accounting for the rigid body rotational motion. The rigid bodies rotational equations of motion are written in a body-fixed frame with the total rigid body rotation matrix updated each time step using incremental rotations.
- Total-Lagrangian lumped parameters 3D finite elements including spring/truss, thin beam, thick beam, thick shell, and solid finite elements.
- Penalty technique for modeling joint constraints including spherical, revolute, cylindrical and prismatic joints.
- Penalty technique for modeling normal contact.
- An asperity friction model is used to model joint and contact friction.
- General fast hierarchical bounding box-bounding sphere contact search algorithm for finding the contact penetration between points on master contact surfaces and polygons on slave contact surfaces.
- Continuous belt-type tracks are modeled using brick elements representing the rubber matrix and beam elements along the width and circumference of the belt/segment for modeling the belt reinforcements.
- Continuous or segmented tracks are modeled thick beam elements.

A validation study of the finite element model was carried out using a tracked vehicle (without the track) mounted on

Unclassified: Distribution Statement A. Appropriate for public release; distribution is unlimited.

an n-post motion simulator. The study shows that the model can predict reasonably well, within 15% difference on average, the response of the vehicle. The maximum difference between the experiments and simulation was 50% for the large frequency excitations, mainly due to the wheels climbing over the dishpan stops in the experiments.

ACKNOWLEDGEMENTS

Support for this work provided by the US Army RDECOM-TARDEC, Warren, MI under SBIR grant number W56HZV05C0631 is gratefully acknowledged.

Reference herein to any specify commercial company, product, process or service by trade name, trademark, manufacturer, or otherwise, does not necessarily constitute or imply its endorsement, recommendation, or favoring by the United States Government or the department of the Army (DoA). The opinions of the authors expressed herein do not necessarily state of reflect those of the United States Government or the DoA, and shall not be used for advertizing or product endorsement purposes.

REFERENCES

[1] T.M. Wasfy and A.K. Noor, "Computational strategies for flexible multibody systems," *Applied Mechanics Reviews*, vol 56(6), pages 553-613, 2003.

[2] T.M. Wasfy and J. O'Kins, "Finite Element Modeling of the Dynamic Response of Tracked Vehicles," ASME DETC 2009-86563, *ASME 2009 International Design Engineering Technical Conferences, 7th International Conference on Multibody Systems, Nonlinear Dynamics, and Control*, San Diego, CA, August 2009.

[3] T.M. Wasfy and A.K. Noor, "Modeling and sensitivity analysis of multibody systems using new solid, shell and beam elements," *Computer Methods in Applied Mechanics and Engineering*, Vol. 138(1-4) (25th Anniversary Issue), pp. 187-211, 1996.

[4] T.M. Wasfy, "Modeling spatial rigid multibody systems using an explicit-time integration finite element solver and a penalty formulation," ASME Paper No. DETC2004-57352, *28th Biennial Mechanisms and Robotics Conference*, DETC, Salt Lake, Utah 2004.

[5] M.J. Leamy and T.M. Wasfy, "Transient and steady-state dynamic finite element modeling of belt-drives," *ASME Journal of Dynamics Systems, Measurement, and Control*, Vol. 124(4), pp. 575-581, 2002.

[6] T.M. Wasfy and M.J. Leamy, "Modeling the dynamic frictional contact of tires using an explicit finite element code," ASME DETC2005-84694, *5th International Conference on Multibody Systems, Nonlinear Dynamics, and Control*, ASME DETC, Long Beach, CA, 2005.

[7] T.M. Wasfy, "Asperity spring friction model with application to belt-drives," Paper No. DETC2003-48343, Proceeding of the DETC: *19th Biennial Conference on Mechanical Vibration and Noise*, Chicago, IL, 2003.

[8] T.M. Wasfy, "A torsional spring-like beam element for the dynamic analysis of flexible multibody systems," *International Journal for Numerical Methods in Engineering*, Vol. 39(7), pp. 1079-1096, 1996.

[9] T.M. Wasfy, "Edge projected planar rectangular element for modeling flexible multibody systems," 19th Biennial Conference on Mechanical Vibration and Noise, Paper No. DETC2003-48351, *19th Biennial Conference on Mechanical Vibration and Noise*, ASME International 2003 DETC, Chicago, IL, 2003.

[10] T.M. Wasfy, "Lumped-parameters brick element for modeling shell flexible multibody systems," *18th Biennial Conference on Mechanical Vibration and Noise*, ASME International 2001 DETC, Pittsburgh, PA, 2001.

Unclassified: Distribution Statement A. Appropriate for public release; distribution is unlimited.